# Bimetallic Pt-Co Nanoparticle Deposited on Alumina for Simultaneous CO and Toluene Oxidation in the Presence of Moisture

*Authors:*

Peng Peng, Jun Li, Shengpeng Mo, Qi Zhang, Taiming Shen, Qinglin Xie

*Abstract:*

Carbon monoxide (CO) and hydrocarbons (HCs) generally have competitive adsorption on the active site of noble-metal nano-catalysts, thus developing an effective way to reduce the passivation of competitive reaction with each other is an urgent problem. In this study, we successfully synthesized transition metal-noble metal (Pt-M) alloys via introducing inexpensive metal elements (M = Ni, Co and Cu) into Pt particles and then deposited on alumina support to form Pt-based catalysts. Subsequently, we choose CO and toluene as polluting gases to evaluate the catalytic activities of Pt-M/Al2O3 catalysts. Introducing inexpensive metal elements (M = Ni, Co, and Cu) significantly changed the physicochemical properties and catalytic activities of these Pt-based catalysts. It can be found that the Pt-Co/Al2O3 catalyst exhibited outstanding catalytic activity for CO and toluene oxidation under mixed gas atmosphere, compared with other Pt-based catalysts, which is due to the higher dispersity, more surface adsorption oxygen, and well redox ability. Surprisingly, H2O could promote the catalytic activities for CO/toluene co-oxidation over the Pt-Co/Al2O3 catalyst. Thus, the present synthetic strategy not only opens an avenue towards the synthesis of noble metal-based catalysts, but also provides an excellent tolerance to H2O in the catalytic process.

*Article*

# Bimetallic Pt-Co Nanoparticle Deposited on Alumina for Simultaneous CO and Toluene Oxidation in the Presence of Moisture

Peng Peng [1], Jun Li [1], Shengpeng Mo [1,2,*], Qi Zhang [2], Taiming Shen [1] and Qinglin Xie [1,*]

[1] College of Environment Science and Engineering, Guilin University of Technology, Guilin 541004, China; pengpeng2017135@163.com (P.P.); lijungute@163.com (J.L.); shentaiming1@163.com (T.S.)

[2] School of Environment and Energy, South China University of Technology, Guangzhou 510006, China; 201720142241@mail.scut.edu.cn

\* Correspondence: moshengpeng14@mails.ucas.ac.cn (S.M.); xqinglin@hotmail.com (Q.X.)

**Abstract:** Carbon monoxide (CO) and hydrocarbons (HCs) generally have competitive adsorption on the active site of noble-metal nano-catalysts, thus developing an effective way to reduce the passivation of competitive reaction with each other is an urgent problem. In this study, we successfully synthesized transition metal-noble metal (Pt-M) alloys via introducing inexpensive metal elements (M = Ni, Co and Cu) into Pt particles and then deposited on alumina support to form Pt-based catalysts. Subsequently, we choose CO and toluene as polluting gases to evaluate the catalytic activities of Pt-M/Al$_2$O$_3$ catalysts. Introducing inexpensive metal elements (M = Ni, Co, and Cu) significantly changed the physicochemical properties and catalytic activities of these Pt-based catalysts. It can be found that the Pt-Co/Al$_2$O$_3$ catalyst exhibited outstanding catalytic activity for CO and toluene oxidation under mixed gas atmosphere, compared with other Pt-based catalysts, which is due to the higher dispersity, more surface adsorption oxygen, and well redox ability. Surprisingly, H$_2$O could promote the catalytic activities for CO/toluene co-oxidation over the Pt-Co/Al$_2$O$_3$ catalyst. Thus, the present synthetic strategy not only opens an avenue towards the synthesis of noble metal-based catalysts, but also provides an excellent tolerance to H$_2$O in the catalytic process.

**Keywords:** bimetallic alloy; Pt-based catalysts; catalytic oxidation; toluene; moisture

## 1. Introduction

In recent years, with the progress of industrial development and the increased number of vehicles, the concentration of carbon monoxide (CO) and hydrocarbons (HCs) in ambient air is on the rise, causing the frequent occurrence of photochemical smog pollution in some areas and seriously threatening people's health [1–9]. However, controlling CO and HCs exhaust emissions can be an important direction to reducing air pollution. At present, there are many technical methods for controlling volatile organic compounds (VOCs), such as adsorption, catalytic oxidation, combustion, plasma, and so on. Among them, catalytic oxidation is known as the most efficient and economical method to remove VOCs [10–14]. Besides, catalytic oxidation has also been recognized as a promising technology for reducing exhaust gases because it directly converts pollutions into CO$_2$ and H$_2$O at relatively lower temperatures and reduces the production of other atmospheric pollutants. Precious metal catalysts and non-precious metal oxide catalysts are the most studied catalytic materials for CO and VOCs oxidation, but Pt-based catalysts are the preferred candidates due to their excellent catalytic properties [15,16]. To date, the commercial 3-way (Pt-Pd-Rh) catalysts have been widely used in the after-treatment system, but the catalytic converters realize the complete removal of CO and HCs exhaust emission at a high-temperature range (300–400 °C) [17]. Significantly, CO and HCs have competitive adsorption on the active sites of catalysts, and the catalytic performance of noble metal catalysts for CO oxidation

can be strongly inhibited when HCs are introduced into the mixed gas [18–21]. For example, Ye et al. [21] synthesized a series of Pt-supported catalysts (Pt-Al$_2$O$_3$, Pt-Co$_3$O$_4$, and Pt-CeO$_2$) for simultaneous CO and toluene oxidation. They found that CO gas was vented into the reactor. The catalytic activities of CO and toluene over the Pt-based catalysts obviously decreased compared to those under individual CO and toluene oxidation due to competitive adsorption on the same active sites. Therefore, it is still an important topic to develop effective ways to reduce the competitive reaction between CO and HCs in Pt-based catalysts.

Recently, many studies have suggested that noble metals and other less expensive metal elements synthesize metal nanoalloys, which not only minimizes the total used amount of precious metals, but also gives rise to a superior catalytic activity due to the rearrangement of the valence electrons in the new potential fields [22–28]. For example, Yang et al. [25] reported that bimetallic Cu-Pd nanoalloys with atomic dispersion supported on aluminum oxide (Al$_2$O$_3$) substrates were applied for oxidizing benzene. The Al$_2$O$_3$-supported Cu-Pd particles with the ratio of Pd to Cu was 0.2 to 1, which exhibited the highest TOF for benzene transformation and the high dispersity of Pd in CuO. Yim et al. [27] also synthesized bimetallic Pt-based (Meso-PtM; M = Ni, Fe, Co, Cu) nanoparticles with self-supported meso-structures that showed very high redox reaction performance and durableness, in which the transition metals (M) promoted oxygen reduction reaction (ORR) activity by modulating the electronic structure and lattice strain. The commercial Pt/C and Pt black catalysts underwent a drastic activity decrease after durability tests, whereas Meso-PtNi with intermetallic phase exhibited superior activity and durability. Besides, Sato et al. [28] also prepared a γ-Al$_2$O$_3$-supported Pt-Co bimetallic catalyst [Pt(0.1)Co(1)/Al$_2$O$_3$] for purification of automotive exhaust, the electron-rich Pt and metallic Co promoted the adsorption and activation steps of the reactions with NO, CO, and hydrocarbons. Therefore, it is ideal for studying bimetallic Pt-based catalysts via introducing inexpensive metal elements for CO and toluene oxidation.

In this work, we reported a facile synthetic strategy to form bimetallic Pt-M (M = Ni, Co and Cu) catalysts for simultaneous CO and toluene oxidation, in which both transition metal and noble Pt metal were introduced onto an alumina support. The structural information of Pt-M/Al$_2$O$_3$ catalysts was further investigated by powder X-ray diffraction (XRD), transmission electron microscopy (TEM), CO-pulse chemisorption, X-ray photoelectron spectroscopy (XPS), hydrogen temperature-programmed reduction (H$_2$-TPR), and oxygen temperature-programmed desorption (O$_2$-TPD) measurement. At the same time, the effect of weight hourly space velocity (WHSV) and moisture, stability test on the catalytic performances of CO/toluene co-oxidation were further investigated. After introducing a secondary inexpensive metal, the catalytic activities over bimetallic Pt-M (M = Ni, Co, Cu) catalysts for CO/toluene oxidation were not significantly decreased. Interestingly, the catalytic activity of only Pt-Co/Al$_2$O$_3$ catalyst was better than that of Pt/Al$_2$O$_3$ catalyst for individual CO and toluene oxidation. When CO and toluene gases simultaneously exist in the reaction gases stream, the catalytic activities of these catalysts for CO and toluene oxidation decreased because of the competing adsorption in the same active sites. In addition, H$_2$O promoted the catalytic activities for CO/toluene oxidation over the Pt-Co/Al$_2$O$_3$ catalyst.

## 2. Experimental Section

### *Synthesis of Pt/Al$_2$O$_3$ Catalyst*

The 2.0 g alumina (γ-Al$_2$O$_3$, ~300 m$^2$ g$^{-1}$, size about 200 nm) powders from Aladdin Reagents (Shanghai, China) and 1.0 mL Platinum nitrate (10.0 mg/mL Pt) were added to 250 mL of ultrapure water. The solution was heated to boiling point under vigorous magnetic stirring. Then, 11.0 mL mixed solution of 1.0 wt.% sodium citrate and 0.05 wt.% citric acid were added to the reaction system. After half a minute, 5.5 mL of a newly synthesized sodium borohydride (0.08 wt.%) solution with 1.0 wt.% sodium citrate and 0.05 wt.% citric acid were added. The above reaction solution was kept at 100 °C for 0.5 h

under vigorous magnetic stirring. After the above process was finished, the solution was cooled to room temperature, washed 3 times with deionized water and ethanol under high-speed centrifugation, and dried at 80 °C for 12 h. Finally, the as-obtained products were reduced by passing 10% $H_2$ at 300 °C for 5 h. The nominal Pt content of $Pt/Al_2O_3$ is 0.5 wt.%. The as-prepared catalyst was denoted as $Pt/Al_2O_3$.

Synthesis of bimetallic $Pt-M/Al_2O_3$ catalysts, sample characterizations, and catalytic oxidation of CO/toluene are presented in the Supplementary material.

## 3. Results and Discussion

### 3.1. XRD Analysis

The XRD patterns of as-synthesized $Pt/Al_2O_3$ and $Pt-M/Al_2O_3$ samples are shown in Figure S1. From the XRD spectra of four samples, it can be seen that each sample contains four distinct diffraction peaks at 37.6°, 45.8°, 39.5°, and 66.8°, corresponding to the (311), (222), (400), and (440) planes of $\gamma$-$Al_2O_3$ (JCPDS card No. 29-0063), respectively. No new diffraction peak corresponding to the Pt or $PtO_x$ phase (approximately 33° and 44°) is observed, and there are no peaks associated with the Pt species. This may be due to the lower loading of Pt species or the high dispersion of Pt particles in the form of small particles on the alumina.

### 3.2. Surface Area Analysis

Figure 1 displays the $N_2$ sorption isotherms and pore size distributions for as-synthesized $Al_2O_3$, $Pt/Al_2O_3$, and $Pt-M/Al_2O_3$ catalysts. Prior to testing, these pristine samples were desorbed at 150 °C for 6.0 h under vacuum. The isotherms in Figure 1a were consistent with type IV isotherms with an H3-type hysteresis loop, indicating a mesoporous structure. The pores of these samples can be seen from the distribution of pore size in Figure 1b. It suggests that each sample is a mesoporous material. The mesoporous structure data of all the samples are summarized in Table 1. The samples have larger surface areas in the range of 205.99 ~ 303.34 $m^2$ $g^{-1}$. Compared to the $Al_2O_3$ support, it can be found that the surface areas of $Pt/Al_2O_3$ and $Pt-M/Al_2O_3$ catalysts decreased slightly, and the pore volumes also decreased slightly between 0.91 $cm^3$ $g^{-1}$ and 0.73 $cm^3$ $g^{-1}$. It is worth noting that pure $Al_2O_3$ possessed the largest surface area and pore volume among all the samples. The reason for this result may be that metal particles on the surface of $Pt/Al_2O_3$ and $Pt-M/Al_2O_3$ catalysts may hinder the pore channel of $Al_2O_3$ support. It is well known that the surface area has an effect on the catalytic activity of most reactions, and the catalysts with larger surface areas have better catalytic activity. In addition, abundant pore structure will be more favorable for the exposure of active sites, thereby facilitating the adsorption and reaction of reactants. However, for these $Pt-M/Al_2O_3$ catalysts, the surface area and pore structure may not be the crucial factors in the CO/toluene oxidation.

### 3.3. Microstructure

It is believed that the particle sizes and dispersions of Pt nanoparticles are also pivotal factors to influence the catalytic properties of these catalysts. Transmission electron microscopy (TEM) measurement was carried out to further reveal microstructures of $Pt/Al_2O_3$ and $Pt-M/Al_2O_3$ samples, as shown in Figure 2. Insets show the size distributions of Pt-based nanoparticles in Figure 2a–d, with the nanoparticles uniformly distributed on the surface of catalysts. These particles calculated from the histograms in Figure 2 have average diameters of ca. 3.5 ± 0.2 nm, ca. 3.6 ± 0.2 nm, ca. 3.5 ± 0.2 nm, and ca. 4.4 ± 0.2 nm for the $Pt/Al_2O_3$, $Pt-Ni/Al_2O_3$, $Pt-Co/Al_2O_3$, $Pt-Cu/Al_2O_3$, respectively. The representative high-resolution TEM (HRTEM) image of $Pt/Al_2O_3$ (Figure 2e) clearly reveals that the surface lattice spacing is measured to be 0.215 nm, which is matched well with the (111) crystal face of Pt phase. For the $Pt-Ni/Al_2O_3$ catalyst, the surface lattice spacing of 0.200 nm is measured in Figure 2f, which is consistent with the (111) lattice plane of Pt. The HRTEM image of $Pt-Co/Al_2O_3$ shows the surface lattice spacing in Figure 2g, and the measured d-spacing is 0.260 nm, consistent with the (200) lattice plane of Pt. For the

Pt-Cu/Al$_2$O$_3$ catalyst (Figure 2d,h), there is the surface lattice spacing with a d-spacing of 0.230 nm, which is matched well with the (200) crystal plane of the Pt phase. From the TEM/HRTEM images of all the catalysts, introducing inexpensive metal elements (M = Ni, Co, Cu) could be used to control the average size of metal Pt nanoparticles. In addition, MO$_x$ phases are not observed, which is due to the lower loading or the formation of intermetallic compounds between Pt and MO$_x$.
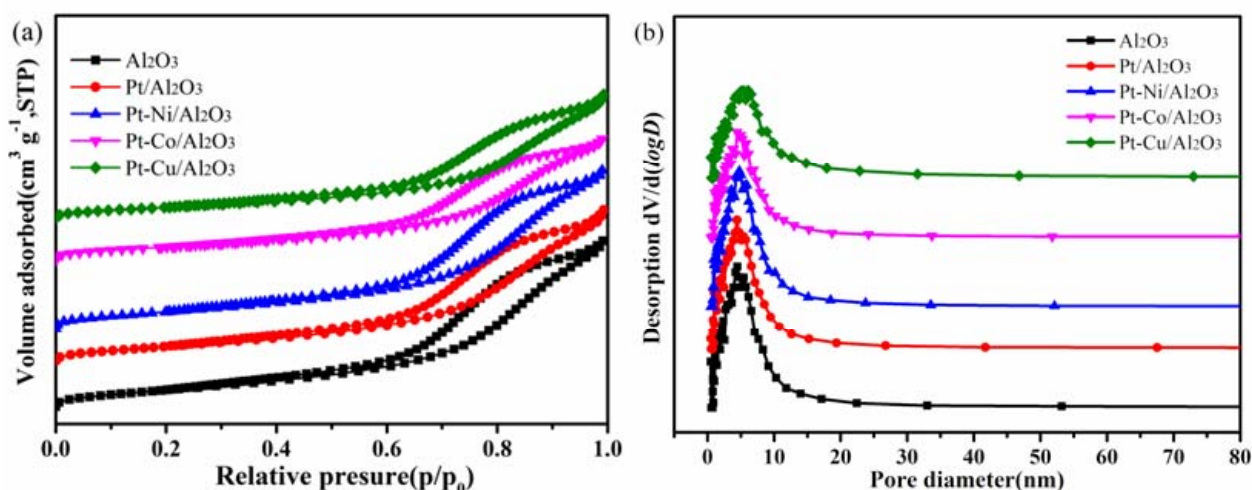


**Figure 1.** (**a**) N$_2$ adsorption/desorption isotherms and (**b**) pore-size distributions for Al$_2$O$_3$, Pt/Al$_2$O$_3$, and Pt-M/Al$_2$O$_3$ samples.

**Table 1.** Elemental compositions, surface area data, and other physical-chemical parameters of Pt-Al$_2$O$_3$ and Pt/M-Al$_2$O$_3$ samples.

| Sample | Pt Loading (wt.%) | M (Ni, Co and Cu) Loading (wt.%) | S$_{BET}$ (m$^2$ g$^{-1}$) | V$_{pore}$ (cm$^3$ g$^{-1}$) | Pore Diameter (nm) | Pt [a] Dispersion (%) | TOF$_{Pt-CO}$ [b] (10$^{-2}$ S$^{-1}$) | TOF$_{Pt-toluene}$ [b] (10$^{-4}$ S$^{-1}$) |
|---|---|---|---|---|---|---|---|---|
| Pt-Al$_2$O$_3$ | 0.49 | — | 269.99 | 0.91 | 6.77 | 47.67 | 3.77 | 2.96 |
| Pt/Ni-Al$_2$O$_3$ | 0.47 | 0.41 | 295.81 | 0.95 | 6.43 | 51.07 | 4.86 | 3.40 |
| Pt/Co-Al$_2$O$_3$ | 0.48 | 0.43 | 226.25 | 0.73 | 6.44 | 59.97 | 5.29 | 4.77 |
| Pt/Cu-Al$_2$O$_3$ | 0.48 | 0.44 | 205.99 | 0.75 | 7.25 | 52.63 | 3.60 | 2.86 |
| Al$_2$O$_3$ | — | — | 303.34 | 1.00 | 6.62 | — | — | — |

[a] Pt dispersion was determined from CO-pulse chemisorption (the CO/Pt ratio is 1.0); [b] The turnover frequency (TOF) values were calculated via the CO/toluene conversions at 190 °C during the mixture conditions.

### 3.4. Temperature Programmed Reduction (TPR)

In Figure 3, the H$_2$-TPR results describe different forms and reduction behaviors of these Pt-based samples. Guo et al. reported that Pd/Al$_2$O$_3$ possessed negative peaks that were corresponded to the decomposition of the β-PdH phase, confirmed the existence of metallic Pd nanoparticles [29,30]. In addition, the H$_2$ desorption peak at higher temperatures indicates that some Pd species are easily reduced at normal temperature. In this work, H$_2$-TPR results show that one negative peak was observed at about 70–100 °C, and one positive peak was detected at about 450–500 °C for these catalysts. Fu et al. [31] revealed that many Co oxide species loaded onto Pt NPs to form a nanoalloy can be reduced at 100 °C. Regalbuto et al. [32] reported that alloying Pt-M (Co, Ni, Cu) was enabled to observe hydrogen spillover. Thus, the negative peak could be the characteristic peak of hydrogen desorption due to the effect of metal Pt particles. The positive peak at high temperatures

could be attributed to the reduction of lattice oxygen species on the surface of $Al_2O_3$. Of course, these positive characteristic peaks at about 450–500 °C can be considered as the reduction peaks of surface lattice oxygen on these catalysts. The above temperature regions of $H_2$ desorption peak over Pt-M/$Al_2O_3$ catalysts are similar to those of Pd/$Al_2O_3$ catalysts reported by Guo et al. [30]. Among these catalysts, the negative peak over the Pt-Co/$Al_2O_3$ catalyst slightly shifted to a higher temperature (93 °C), manifesting that the Pt species in Pt-Co/$Al_2O_3$ catalyst could still be easily reduced at lower temperatures. In addition, the addition of transition metal can cause the reduction peak to move slightly, and the intensity of hydrogen consumption at about 450–500 °C on the Pt-M/$Al_2O_3$ catalysts is obviously decreased, which is mainly caused by the electronic interaction between transition metal oxides ($MO_x$) and Pt nanoparticles.
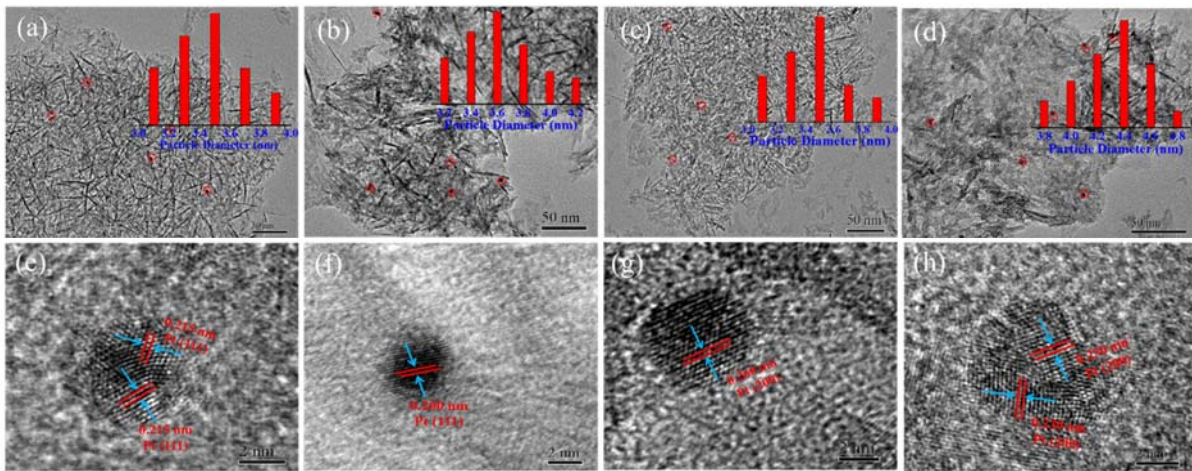


**Figure 2.** (**a**) Pt/$Al_2O_3$, (**b**) Pt-Ni/$Al_2O_3$, (**c**) Pt-Co/$Al_2O_3$, and (**d**) Pt-Cu/$Al_2O_3$, as well as corresponding to (**e**–**h**) high-resolution transmission electron microscopy (HRTEM) images in the (**a**–**d**) TEM images, respectively (insets are the histograms to display the size distributions of Pt-based nanoparticles).
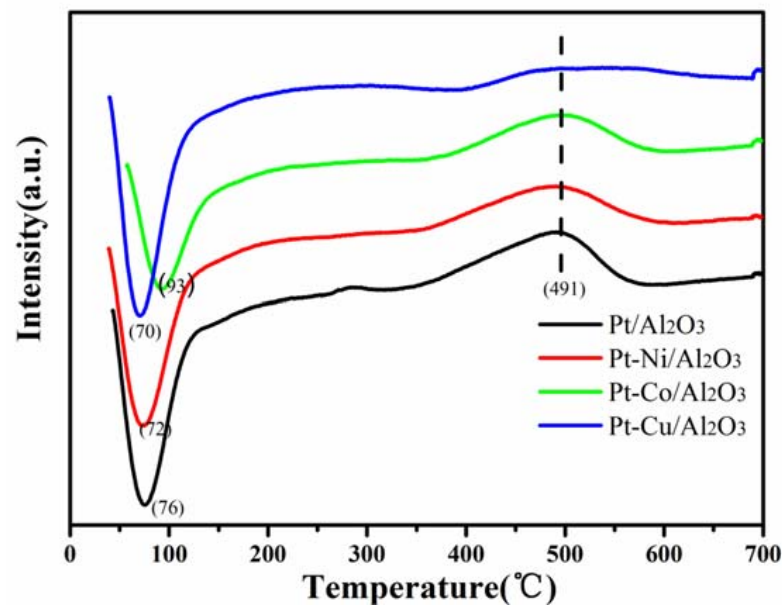


**Figure 3.** $H_2$-TPR profiles of as-synthesized Pt/$Al_2O_3$ and Pt-M/$Al_2O_3$ samples.

### 3.5. Surface Element Composition

To further investigate the surface composition of these Pt-based catalysts, X-ray photo-electron spectra (XPS) measurement was tested on the four samples. Figure 4 illustrates Al 2p/Pt 4f and O1s XPS spectra of all the samples. Since the characteristic peaks of Al 2p and Pt 4f were close and overlapped in the range of 73~75 eV, thus the valency of platinum was not determined from Figure 4a. XPS spectra of O 1s were also further analyzed, and three oxygen chemical states were observed on the surface of Pt-based catalysts, as shown in Figure 4b. Wherein, the main peak with an O 1s spectrum appears in the position of binding energy (BE) of around 531.1 eV, which was related to lattice oxygen species ($O_{latt}$) [33,34]. While the peak at 532.2 eV was considered to be surface absorbed oxygen species ($O_{ads}$), and the weak peak at 533 eV was ascribed to adsorbed hydroxyl and water molecules ($O_{-OH}$). Besides, the proportion of three oxygen chemical states over these samples was calculated, the results are shown in Table 2. The oxygen vacancy ($O_{ads}$ + $O_{-OH}$) ratios were Pt/$Al_2O_3$ (39.1%), Pt-Ni/$Al_2O_3$ (40.3%), Pt-Co/$Al_2O_3$ (42.5%), and Pt-Cu/$Al_2O_3$ (36.4%), respectively, indicating that Pt-Co/$Al_2O_3$ can provide the higher content of surface oxygen species. The existence of oxygen vacancies was of great significance to the chemical properties and catalytic activities of nanomaterials.
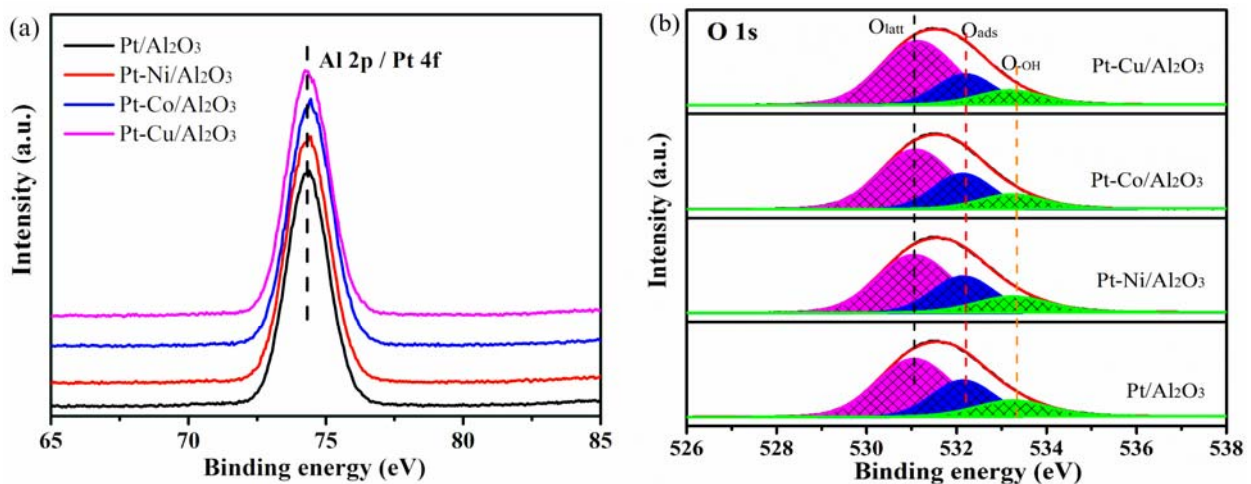


**Figure 4.** (**a**) Al 2p/Pt 4f and (**b**) O1s XPS spectra of these Pt/$Al_2O_3$ and Pt-M/$Al_2O_3$ samples.

**Table 2.** The binding energy and percentage ratio of O 1s XPS results over these Pt-based samples.

| Sample | $O_{latt}$ BE (eV) | $O_{ads}$ BE (eV) | $O_{-OH}$ BE (eV) | $O_{latt}$ (%) | $O_{ads}$ (%) | $O_{OH}$ (%) |
|---|---|---|---|---|---|---|
| Pt/$Al_2O_3$ | 531.17 | 532.23 | 533.41 | 60.9 | 23 | 16.1 |
| Pt-Ni/$Al_2O_3$ | 531.06 | 532.24 | 533.4 | 59.7 | 27.0 | 13.3 |
| Pt-Co/$Al_2O_3$ | 531.08 | 532.13 | 533.23 | 57.5 | 27.3 | 15.2 |
| Pt-Cu/$Al_2O_3$ | 531.13 | 532.19 | 533.18 | 63.6 | 23.2 | 13.2 |

### 3.6. Oxygen Temperature-Programmed Desorption ($O_2$-TPD)

$O_2$-TPD experiments were performed to understand their $O_2$ desorption behavior, as shown in Figure 5. Three distinct desorption peaks could be seen on four catalysts, corresponding to different desorption oxygen species. The conversion process of oxygen adsorption on a catalyst was followed [35–37]: $O_2$ (ads) → $O_2^-$ (ads) → $O^{2-}$ (ads) → $O^{2-}$ (latt). Thus, it can be seen that these different states of oxygen on the surface of catalysts. Three distinct peaks were observed at about 170 ~ 210 °C, 400 ~ 420 °C, and 500 ~ 550 °C. A α strong peak in the range of 100 ~ 300 °C was regarded as the physically surface-adsorbed oxygen species and adsorbed $O_2^-$ species (ads-$O_2$ and ads-$O_2^-$, respectively) [36,38,39]. A β peak in between 300 and 450 °C was assigned to surface lattice species (latt-$O^{2-}$), while

the third peak ($\gamma$ peak in between 450 and 600 °C) belongs to the pyrolysis of lattice oxygen at high temperature [40]. If the catalyst with $\alpha$ peak at a lower temperature level indicated that there could be more likely to produce surface oxygen species, which will provide higher catalytic activity. Generally speaking, a material with abundant reactive oxygen species can perform a redox reaction at lower temperatures, and the high-temperature oxygen fluidity can improve the efficiency of transporting oxygen species. As everyone knows that the oxidation process of VOCs mainly follows a Mars–van Krevelen mechanism and the reaction occurs due to a nucleophilic attack of surface absorbed oxygen species [41,42]. Meanwhile, the higher levels of surface active-oxygen species were conducive to VOCs oxidation [40,43–45]. Abundant surface oxygen vacancies could facilitate the formation of surface adsorbed oxygen species, which was verified by measuring the higher oxygen vacancy molar ratios of catalysts via XPS results in this study. Therefore, the strong desorption peak ($\alpha$ peak) of Pt-Co/$Al_2O_3$ suggests that more surface adsorption oxygen can be provided by the Pt-Co/$Al_2O_3$ catalyst, resulting in the catalytic performance of CO/toluene oxidation being improved significantly.
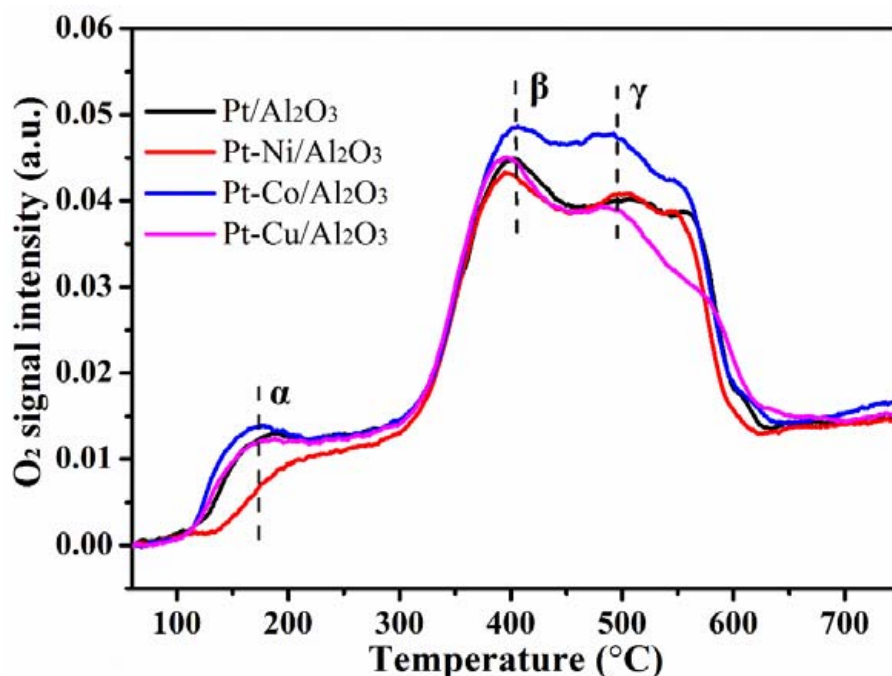


**Figure 5.** $O_2$-TPD profiles of these Pt/$Al_2O_3$ and Pt-M/$Al_2O_3$ samples.

*3.7. Catalytic Activity Measurement*

Figure 6 shows the catalytic activities for CO/toluene of Pt-based samples under different reaction conditions as a function of temperature, while the CO/toluene conversion plots were recorded at the heat preservation stage for 1.0 h. $CO_2$ and $H_2O$ were the main products, while other by-products (below 1.0 ppm) were not detected. The catalytic activities of these samples were compared by using $T_{10}$, $T_{50}$, and $T_{99}$ (the catalytic temperatures of 10%, 50%, and 99% CO/toluene conversion, respectively) as a reference, as described in Table 3. It can be found that all the catalysts have more outstanding catalytic activities than Pt/$Al_2O_3$ ($T_{99}$ = 180 °C) for individual CO oxidation in Figure 6a, their $T_{99}$ values for CO oxidation were achieved at 160 °C with a WHSV of 60,000 mL $g^{-1}$ $h^{-1}$. For individual toluene oxidation, Pt-Co/$Al_2O_3$ catalyst exhibited an optimal catalytic activity among these Pt-based catalysts in Figure 6b, its $T_{10}$, $T_{50}$, $T_{99}$ are 160, 180, and 195 °C, respectively. However, the catalytic performance of bimetallic Pt-Ni/$Al_2O_3$ and Pt-Cu/$Al_2O_3$ catalysts for toluene oxidation was reduced, compared with the Pt/$Al_2O_3$ catalyst. However, when CO and toluene gases simultaneously exist in the reaction gases stream, the catalytic activities for CO and toluene oxidation over all the catalysts were inhibited due to the

competitive adsorption of CO and toluene on the same active sites, as shown in Figure 6c and d. In addition, it can be found that there was an inverse hysteresis in CO or toluene conversion during catalytic oxidation over Pt-Co/Al$_2$O$_3$ catalyst in Figure S2, which was due to exothermic combustion. The Pt/Al$_2$O$_3$ catalyst exhibited complete oxidation for CO and toluene co-existence at 200 °C. Among bimetallic Pt-M/Al$_2$O$_3$ catalysts, Pt-Co/Al$_2$O$_3$ catalyst exhibited a more excellent catalytic activity for CO and toluene oxidation in mixture conditions, while Pt-Ni/Al$_2$O$_3$ and Pt-Cu/Al$_2$O$_3$ catalysts displayed a poorer CO and toluene oxidation activity than the Pt/Al$_2$O$_3$ catalyst. The presence of toluene caused an obvious decrease in CO conversion due to competitive adsorption of both CO and toluene on the surface of catalysts. Moreover, Platinum atoms exposed on the surface of catalytic materials were often considered as the active site for controlling the catalytic oxidation of CO/toluene. The TOF values for CO/toluene co-oxidation at 190 °C have also been calculated in Figure 7. With the increased dispersity of Pt in bimetallic catalysts, the Pt-based catalysts would effectively increase the catalytic activity and TOF of each active site. Therefore, the Pt-Co/Al$_2$O$_3$ catalyst with the highest dispersity and TOF value exhibited the best catalytic performances for CO/toluene oxidation at a lower temperature.
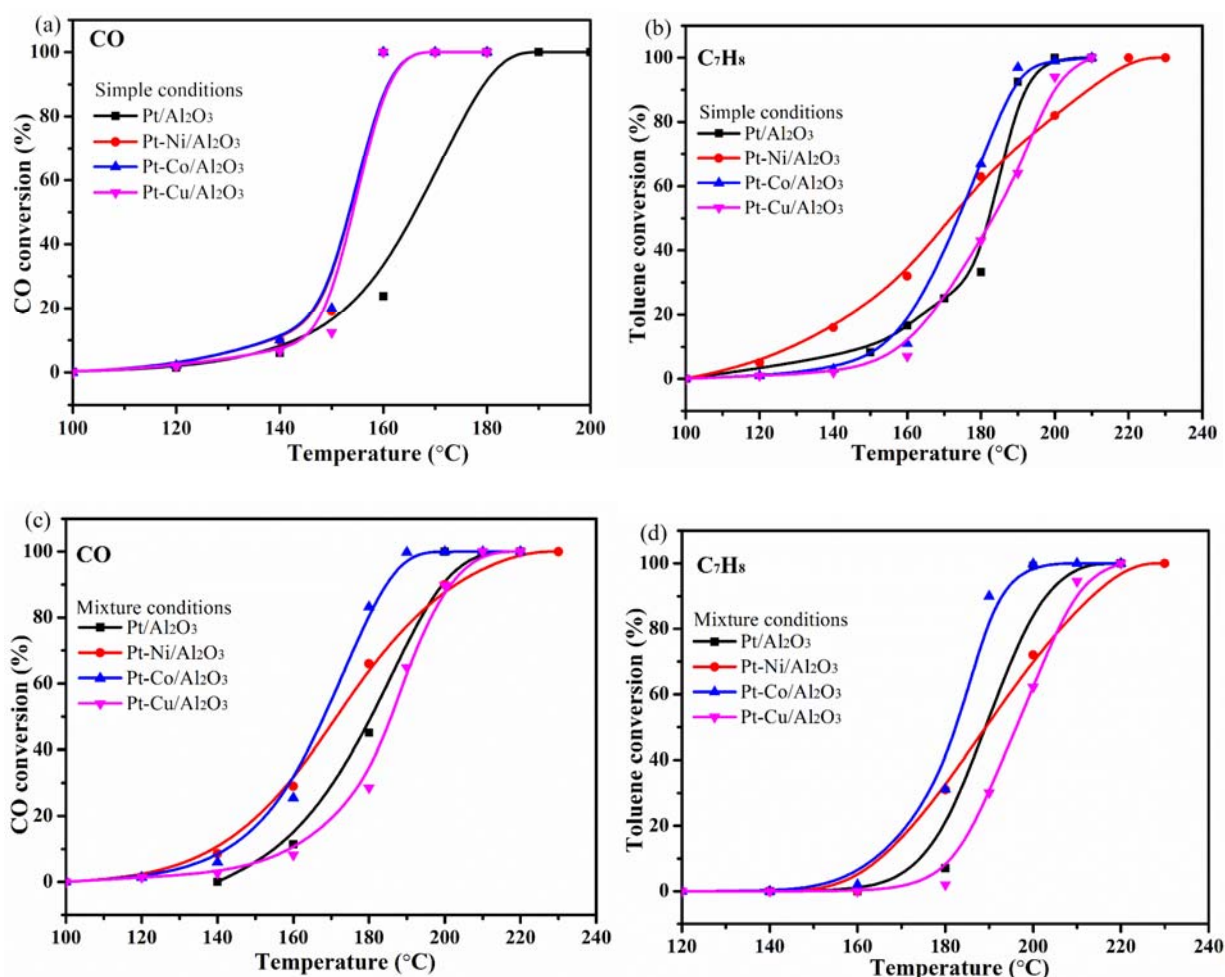


**Figure 6.** (**a**) CO and (**b**) toluene conversions in simple conditions of these Pt/Al$_2$O$_3$ and Pt-M/Al$_2$O$_3$ samples; (**c**) CO and (**d**) toluene conversion in mixture conditions of these Pt/Al$_2$O$_3$ and Pt-M/Al$_2$O$_3$ samples. Simple conditions: 1.0 vol.% CO or 1000 ppm toluene balanced with air; Mixture conditions: 1.0 vol.% CO and 1000 ppm toluene balanced with air. All the reactions were kept at WHSV = 60,000 mL g$^{-1}$ h$^{-1}$.

**Table 3.** Catalytic activities of these $Pt/Al_2O_3$ and $Pt-M/Al_2O_3$ samples under different conditions.

| Sample | Temperature (°C) | Simple Conditions | | | Mixture Conditions | | |
|---|---|---|---|---|---|---|---|
| | | $T_{10}$/°C | $T_{50}$/°C | $T_{99}$/°C | $T_{10}$/°C | $T_{50}$/°C | $T_{99}$/°C |
| $Pt/Al_2O_3$ | CO | 144 | 169 | 180 | 155 | 180 | 200 |
| | Toluene | 150 | 182 | 200 | 176 | 190 | 200 |
| $Pt-Ni/Al_2O_3$ | CO | 140 | 155 | 160 | 139 | 172 | 220 |
| | Toluene | 130 | 172 | 220 | 166 | 190 | 220 |
| $Pt-Co/Al_2O_3$ | CO | 140 | 155 | 160 | 142 | 168 | 190 |
| | Toluene | 153 | 174 | 195 | 165 | 182 | 200 |
| $Pt-Cu/Al_2O_3$ | CO | 143 | 156 | 160 | 160 | 185 | 210 |
| | Toluene | 158 | 185 | 210 | 182 | 198 | 220 |
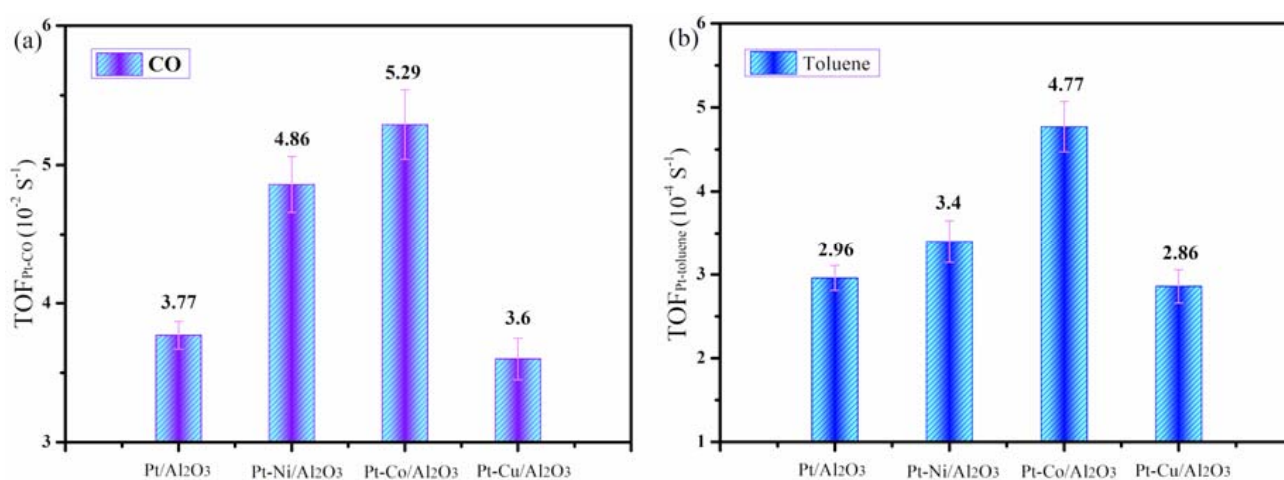


**Figure 7.** The TOF values for (**a**) CO and (**b**) toluene oxidation over these $Pt/Al_2O_3$ and $Pt-M/Al_2O_3$ samples at 190 °C under mixture conditions.

### 3.8. The Effects of WHSV and Moisture

The effect of WHSV on the catalytic activities of $Pt-Co/Al_2O_3$ catalyst for CO/toluene oxidation was further investigated, as shown in Figure 8. With the increase in WHSV values, the catalytic activities of CO/toluene oxidation decreased. Under the condition of WHSV = 30,000 mL g$^{-1}$ h$^{-1}$, the temperature of complete oxidation for individual CO and toluene oxidation could be obtained at a temperature of 160 and 190 °C, respectively, whereas the $T_{99}$ values for CO and toluene oxidation in mixture conditions were about 170 and 190 °C, respectively. When the WHSV value was further increased to 120,000 mL g$^{-1}$ h$^{-1}$, the $Pt-Co/Al_2O_3$ catalyst can completely degrade the CO and toluene at below 220 °C.

To simulate more realistic conditions, certain moisture was introduced into the simulated off-gas stream, which could obviously affect the catalytic performance of catalyst. The influence of moisture on the catalytic activities of the $Pt-Co/Al_2O_3$ catalyst for CO/toluene oxidation are showed in Figure 9. Surprisingly, it can be found that $H_2O$ promotes the catalytic activities for CO/toluene oxidation over the $Pt-Co/Al_2O_3$ catalyst. In addition, the promoting effect of $H_2O$ in individual CO/toluene oxidation is more remarkable than that in CO and toluene co-oxidation. For individual CO/toluene oxidation with moisture, $Pt-Co/Al_2O_3$ catalyst maintains full CO and toluene conversions at a temperature of 150 °C and 190 °C, respectively. Under the mixture conditions with moisture, the CO and toluene conversions would be mildly facilitated by moisture. Therefore, it can be seen from the experimental data that the $Pt-Co/Al_2O_3$ catalyst owns an excellent tolerance to $H_2O$ in the oxidation process, and $H_2O$ also have a similar promoting effect on other catalysts [44,46–48].
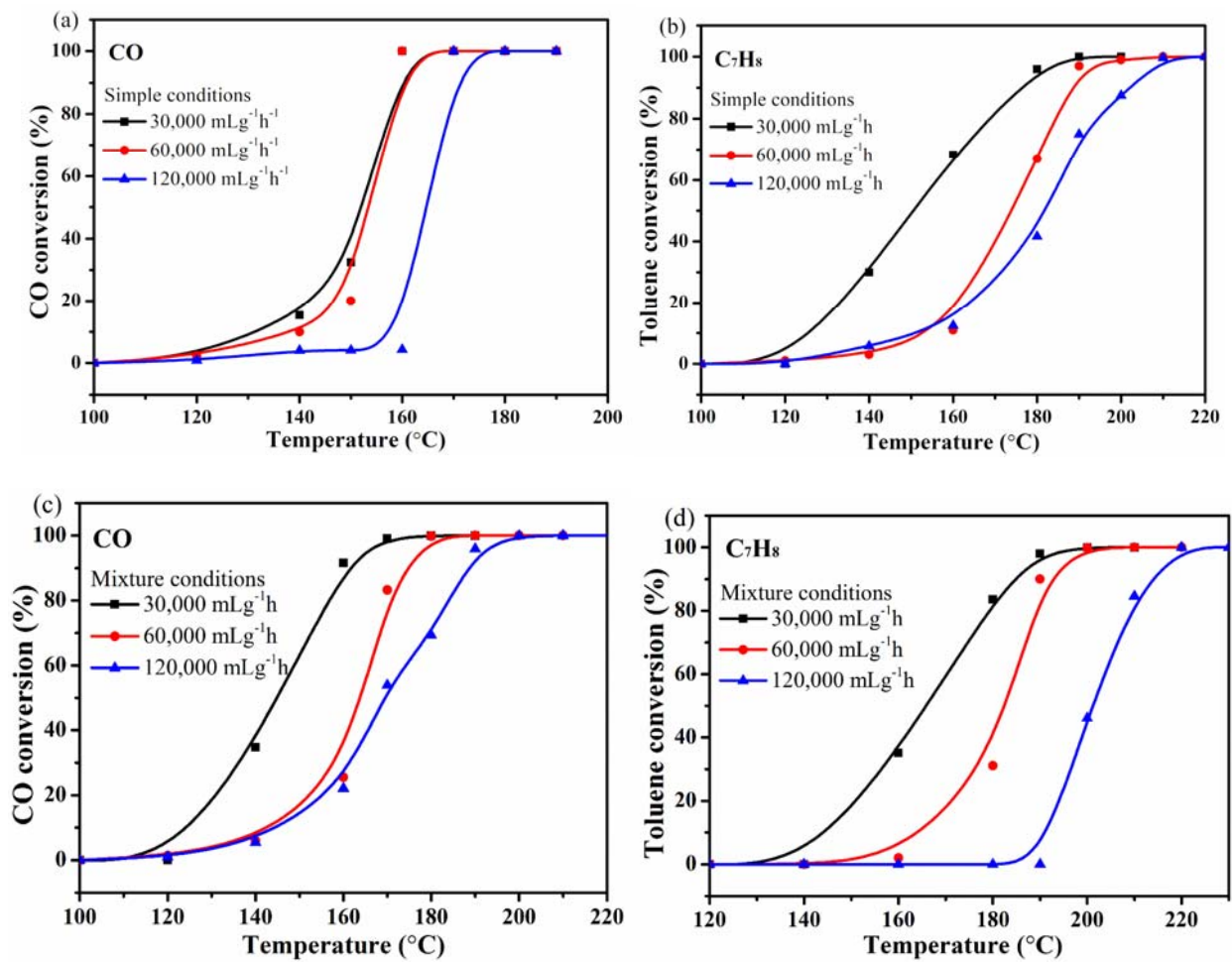
**Figure 8.** (**a**) CO and (**b**) toluene conversions in simple conditions, (**c**) CO and (**d**) toluene conversions in mixture conditions over the Pt-Co/Al$_2$O$_3$ catalyst under different WHSV.
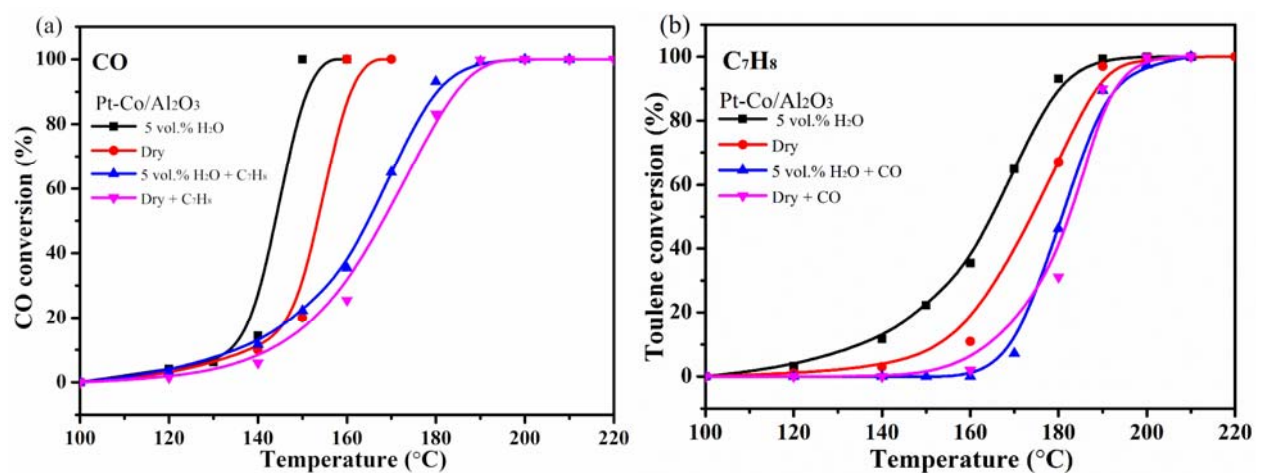


**Figure 9.** The effect of moisture on the (**a**) CO and (**b**) toluene conversions in different conditions over the Pt-Co/Al$_2$O$_3$ catalyst with a weight hourly space velocity (WHSV) = 60,000 mL g$^{-1}$ h$^{-1}$.

### 3.9. Catalytic Stability

Figure S3 shows an on-stream stability experiment for CO/toluene oxidation over the Pt-Co/Al$_2$O$_3$ catalyst at different conditions under a WHSV of 60,000 mL g$^{-1}$ h$^{-1}$. During the long-term stability test for 48 h, the conversions of CO and toluene over the Pt-

$Co/Al_2O_3$ catalyst under dry conditions at a temperature 200 °C were found to be 100% and 98% in Figure S3a, respectively, which were not significantly decreased. Besides, their CO and toluene conversions with or without $H_2O$ under mixture conditions at a temperature of 180 °C did not fluctuate significantly in Figure S3b. The above results manifest that the $Pt-Co/Al_2O_3$ catalyst exhibits a relatively high catalytic activity for CO/toluene oxidation, good stability as well as high resistance to CO and hydrocarbon inhibition in the simulated exhaust stream, indicating that the $Pt-Co/Al_2O_3$ catalyst can be well applied to CO and toluene co-oxidation.

## 4. Conclusions

In summary, we have successfully synthesized bimetallic Pt-M (M = Ni, Co, Cu) on alumina substrates via introducing inexpensive metal elements for the catalytic removal of CO and toluene co-existence. It can be found that introducing inexpensive metal elements into $Pt/Al_2O_3$ catalyst clearly changes the physico-chemical properties, anti-toxic abilities, and catalytic performances for CO and toluene co-oxidation. The catalytic evaluations of CO/toluene oxidation indicate that the $Pt-Co/Al_2O_3$ catalyst exhibits the best catalytic activity for complete CO and toluene oxidation ($T_{99/CO}$ = 160 °C, $T_{99/toluene}$ = 200 °C) under individual atmosphere among these Pt-based catalysts. Moreover, the bimetallic Pt-$M/Al_2O_3$ catalysts display identical catalytic performance ($T_{99/CO}$ = 160 °C) for individual CO oxidation, which is higher than the $Pt/Al_2O_3$ catalyst. For CO and toluene co-oxidation, the $Pt-Co/Al_2O_3$ catalyst also had the lowest temperature, and CO and toluene have competitive adsorption at the active sites of catalysts. Importantly, $H_2O$ promotes the catalytic activities for CO/toluene oxidation over the $Pt-Co/Al_2O_3$ catalyst due to excellent tolerance to $H_2O$. According to the catalytic and characterization analysis, it can be seen that $Pt-Co/Al_2O_3$ catalyst with superior activity has the highest turnover frequency (TOF) for CO/toluene conversion and the well dispersity of Pt particles. In addition, the catalytic performance is related to the Pt particle size, metal species, more surface adsorption oxygen, and well redox ability. However, the pathway introducing Ni and Cu elements into $Pt/Al_2O_3$ to prepare $Pt-Ni/Al_2O_3$ and $Pt-Cu/Al_2O_3$ do not achieve the desired goal of increasing catalytic activity for simultaneous CO and toluene oxidation and the synthesis of Pt-based catalysts decorating a low content of Co metal element is a useful method to improve Pt-metal utilization in the CO and toluene oxidation.

**Conflicts of Interest:** The authors declare no conflict of interest.

## References

1.  Russell, A.; Epling, W.S. Diesel Oxidation Catalysts. *Catal. Rev.* **2011**, *53*, 337–423. [CrossRef]
2.  Feng, X.; Guo, J.; Wen, X.; Xu, M.; Chu, Y.; Yuan, S. Enhancing performance of Co/CeO$_2$ catalyst by Sr doping for catalytic combustion of toluene. *App. Surf. Sci.* **2018**, *445*, 145–153. [CrossRef]
3.  Peng, R.; Li, S.; Sun, X.; Ren, Q.; Chen, L.; Fu, M.; Wu, J.; Ye, D. Size effect of Pt nanoparticles on the catalytic oxidation of toluene over Pt/CeO$_2$ catalysts. *Appl. Catal. B Environ.* **2018**, *220*, 462–470. [CrossRef]
4.  Torrente-Murciano, L.; Solsona, B.; Agouram, S.; Sanchis, R.; López, J.M.; García, T.; Zanella, R. Low temperature total oxidation of toluene by bimetallic Au–Ir catalysts. *Catal. Sci. Technol.* **2017**, *7*, 2886–2896. [CrossRef]
5.  Mo, S.; Li, S.; Ren, Q.; Zhang, M.; Sun, Y.; Wang, B.; Feng, Z.; Zhang, Q.; Chen, Y.; Ye, D. Vertically-aligned Co$_3$O$_4$ arrays on Ni foam as monolithic structured catalysts for CO oxidation: Effects of morphological transformation. *Nanoscale* **2018**, *10*, 7746–7758. [CrossRef]
6.  Wang, H.; Lu, Y.; Han, Y.; Lu, C.; Wan, H.; Xu, Z.; Zheng, S. Enhanced catalytic toluene oxidation by interaction between copper oxide and manganese oxide in Cu-O-Mn/$\gamma$-Al$_2$O$_3$ catalysts. *App. Surf. Sci.* **2017**, *420*, 260–266. [CrossRef]
7.  Chen, J.; Li, Y.; Fang, S.; Yang, Y.; Zhao, X. UV–Vis-infrared light-driven thermocatalytic abatement of benzene on Fe doped OMS-2 nanorods enhanced by a novel photoactivation. *Chem. Eng. J.* **2018**, *332*, 205–215. [CrossRef]
8.  Cheng, L.; Men, Y.; Wang, J.; Wang, H.; An, W.; Wang, Y.; Duan, Z.; Liu, J. Crystal facet-dependent reactivity of $\alpha$-Mn$_2$O$_3$ microcrystalline catalyst for soot combustion. *Appl. Catal. B Environ.* **2017**, *204*, 374–384. [CrossRef]
9.  Li, S.; Wang, D.; Wu, X.; Chen, Y. Recent advance on VOCs oxidation over layered double hydroxides derived mixed metal oxides. *Chin. J. Catal.* **2020**, *41*, 550–560. [CrossRef]
10. Ma, L.; Seo, C.Y.; Chen, X.; Li, J.; Schwank, J.W. Sodium-promoted Ag/CeO$_2$ nanospheres for catalytic oxidation of formaldehyde. *Chem. Eng. J.* **2018**, *350*, 419–428. [CrossRef]
11. Kamal, M.S.; Razzak, S.A.; Hossain, M.M. Catalytic oxidation of volatile organic compounds (VOCs)—A review. *Atmos. Environ.* **2016**, *140*, 117–134. [CrossRef]
12. Mo, S.; Li, S.; Xiao, H.; He, H.; Xue, Y.; Zhang, M.; Ren, Q.; Chen, B.; Chen, Y.; Ye, D. Low-temperature CO oxidation over integrated penthorum chinense-like MnCo$_2$O$_4$ arrays anchored on three-dimensional Ni foam with enhanced moisture resistance. *Catal. Sci. Technol.* **2018**, *8*, 1663–1676. [CrossRef]
13. Mo, S.; Zhang, Q.; Li, S.; Ren, Q.; Zhang, M.; Xue, Y.; Peng, R.; Xiao, H.; Chen, Y.; Ye, D. Integrated Cobalt Oxide Based Nanoarray Catalysts with Hierarchical Architectures: In Situ Raman Spectroscopy Investigation on the Carbon Monoxide Reaction Mechanism. *ChemCatChem* **2018**, *10*, 3012–3026. [CrossRef]
14. Mo, S.; Zhang, Q.; Sun, Y.; Zhang, M.; Li, J.; Ren, Q.; Fu, M.; Wu, J.; Chen, L.; Ye, D. Gaseous CO and toluene co-oxidation over monolithic core–shell Co$_3$O$_4$-based hetero-structured catalysts. *J. Mater. Chem. A* **2019**, *7*, 16197–16210. [CrossRef]
15. Slavinskaya, E.M.; Stadnichenko, A.I.; Muravyov, V.V.; Kardash, T.Y.; Derevyannikova, E.A.; Zaikovskii, V.I.; Stonkus, O.A.; Lapin, I.N.; Svetlichnyi, V.A.; Boronin, A.I. Transformation of a Pt-CeO$_2$ Mechanical Mixture of Pulsed-Laser-Ablated Nanoparticles to a Highly Active Catalyst for Carbon Monoxide Oxidation. *ChemCatChem* **2018**, *10*, 2232–2247. [CrossRef]
16. Mo, S.; Zhang, Q.; Zhang, M.; Zhang, Q.; Li, J.; Fu, M.; Wu, J.; Chen, P.; Ye, D. Elucidating the special role of strong metal–support interactions in Pt/MnO$_2$ catalysts for total toluene oxidation. *Nanoscale Horiz.* **2019**, *4*, 1425–1433. [CrossRef]
17. Zhang, Y.; Cattrall, R.W.; McKelvie, I.D.; Kolev, S.D. Gold, an alternative to platinum group metals in automobile catalytic converters. *Gold Bull.* **2011**, *44*, 145–153. [CrossRef]
18. Dadi, R.K.; Luss, D.; Balakotaiah, V. Bifurcation features of mixtures containing CO and hydrocarbons in diesel oxidation catalyst. *Chem. Eng. J.* **2016**, *304*, 941–952. [CrossRef]
19. Buzková Arvajová, A.; Březina, J.; Pečinka, R.; Kočí, P. Modeling of two-step CO oxidation light-off on Pt/$\gamma$-Al$_2$O$_3$ in the presence of C$_3$H$_6$ and NO$_x$. *Appl. Catal. B Environ.* **2018**, *233*, 167–174. [CrossRef]
20. Ma, L.; Seo, C.Y.; Chen, X.; Sun, K.; Schwank, J.W. Indium-doped Co$_3$O$_4$ nanorods for catalytic oxidation of CO and C$_3$H$_6$ towards diesel exhaust. *Appl. Catal. B Environ.* **2018**, *222*, 44–58. [CrossRef]
21. Zhang, Q.; Mo, S.; Li, J.; Sun, Y.; Zhang, M.; Chen, P.; Fu, M.; Wu, J.; Chen, L.; Ye, D. In situ DRIFT spectroscopy insights into the reaction mechanism of CO and toluene co-oxidation over Pt-based catalysts. *Catal. Sci. Technol.* **2019**, *9*, 4538–4551. [CrossRef]
22. Wen, M.; Yang, D.; Wu, Q.S.; Lu, R.P.; Zhu, Y.Z.; Zhang, F. Inducing synthesis of amorphous EuFePt nanorods and their comprehensive enhancement of magnetism, thermostability and photocatalysis. *Chem. Commun.* **2010**, *46*, 219–221. [CrossRef] [PubMed]
23. Li, X.; Wang, X.; Liu, M.; Liu, H.; Chen, Q.; Yin, Y.; Jin, M. Construction of Pd-M (M = Ni, Ag, Cu) alloy surfaces for catalytic applications. *Nano Res.* **2017**, *11*, 780–790. [CrossRef]
24. Fang, H.; Yang, J.; Wen, M.; Wu, Q. Nanoalloy Materials for Chemical Catalysis. *Adv. Mater.* **2018**, *30*, 1705698–1705707. [CrossRef]
25. Xu, L.; Chen, D.; Qu, J.; Wang, L.; Tang, J.; Liu, H.; Yang, J. Replacement reaction-based synthesis of supported palladium catalysts with atomic dispersion for catalytic removal of benzene. *J. Mater. Chem. A* **2018**, *6*, 17032–17039. [CrossRef]

26. Huang, X.; Zhao, Z.; Cao, L.; Chen, Y.; Zhu, E.; Lin, Z.; Li, M.; Yan, A.; Zettl, A.; Wang, Y.M.; et al. High-performance transition metal–doped Pt$_3$Ni octahedra for oxygen reduction reaction. *Science* **2015**, *348*, 1230–1232. [CrossRef]

27. Kim, H.Y.; Cho, S.; Sa, Y.J.; Hwang, S.M.; Park, G.G.; Shin, T.J.; Jeong, H.Y.; Yim, S.D.; Joo, S.H. Self-Supported Mesostructured Pt-Based Bimetallic Nanospheres Containing an Intermetallic Phase as Ultrastable Oxygen Reduction Electrocatalysts. *Small* **2016**, *12*, 5347–5353. [CrossRef]

28. Sato, K.; Ito, A.; Tomonaga, H.; Kanematsu, H.; Wada, Y.; Asakura, H.; Hosokawa, S.; Tanaka, T.; Toriyama, T.; Yamamoto, T.; et al. Isolated electron-rich Pt at the surface of Pt-Co alloy nanoparticles on γ-Al$_2$O$_3$ support: Synergistic effect between Pt and Co for exhaust purification. *ChemPlusChem* **2019**, *84*, 447–456. [CrossRef]

29. Shen, W.-J.; Okumura, M.; Matsumura, Y.; Haruta, M. The influence of the support on the activity and selectivity of Pd in CO hydrogenation. *Appl. Catal. A Gen.* **2001**, *213*, 225–232. [CrossRef]

30. Zhang, Y.; Cai, Y.; Guo, Y.; Wang, H.; Wang, L.; Lou, Y.; Guo, Y.; Lu, G.; Wang, Y. The effects of the Pd chemical state on the activity of Pd/Al$_2$O$_3$ catalysts in CO oxidation. *Catal. Sci. Technol.* **2014**, *4*, 3973–3980. [CrossRef]

31. Xu, X.; Fu, Q.; Wei, M.; Wu, X.; Bao, X. Comparative studies of redox behaviors of Pt–Co/SiO$_2$ and Au–Co/SiO$_2$ catalysts and their activities in CO oxidation. *Catal. Sci. Technol.* **2014**, *4*, 3151–3158. [CrossRef]

32. Wong, A.; Liu, Q.; Griffin, S.; Nicholls, A.; Regalbuto, J.R. Synthesis of ultrasmall, homogeneously alloyed, bimetallic nanoparticles on silica supports. *Science* **2017**, *358*, 1427–1430. [CrossRef] [PubMed]

33. Tang, W.; Xiao, W.; Wang, S.; Ren, Z.; Ding, J.; Gao, P.-X. Boosting catalytic propane oxidation over PGM-free Co$_3$O$_4$ nanocrystal aggregates through chemical leaching: A comparative study with Pt and Pd based catalysts. *Appl. Catal. B Environ.* **2018**, *226*, 585–595. [CrossRef]

34. Chen, X.; Chen, X.; Yu, E.; Cai, S.; Jia, H.; Chen, J.; Liang, P. In situ pyrolysis of Ce-MOF to prepare CeO$_2$ catalyst with obviously improved catalytic performance for toluene combustion. *Chem. Eng. J.* **2018**, *344*, 469–479. [CrossRef]

35. Wang, Y.-Z.; Zhao, Y.-X.; Gao, C.-G.; Liu, D.-S. Origin of the High Activity and Stability of Co$_3$O$_4$ in Low-temperature CO Oxidation. *Catal. Lett.* **2008**, *125*, 134–138. [CrossRef]

36. Jha, A.; Mhamane, D.; Suryawanshi, A.; Joshi, S.M.; Shaikh, P.; Biradar, N.; Ogale, S.; Rode, C.V. Triple nanocomposites of CoMn$_2$O$_4$, Co$_3$O$_4$ and reduced graphene oxide for oxidation of aromatic alcohols. *Catal. Sci. Technol.* **2014**, *4*, 1771. [CrossRef]

37. Zhao, W.; Zhang, Y.; Wu, X.; Zhan, Y.; Wang, X.; Au, C.-T.; Jiang, L. Synthesis of Co-Mn oxides with double-shelled nanocages for low-temperature toluene combustion. *Catal. Sci. Technol.* **2018**, *8*, 4494–4502. [CrossRef]

38. Zhang, Q.; Liu, X.; Fan, W.; Wang, Y. Manganese-promoted cobalt oxide as efficient and stable non-noble metal catalyst for preferential oxidation of CO in H$_2$ stream. *Appl. Catal. B Environ.* **2011**, *102*, 207–214. [CrossRef]

39. Zhang, Q.; Mo, S.; Chen, B.; Zhang, W.; Huang, C.; Ye, D. Hierarchical Co$_3$O$_4$ nanostructures in-situ grown on 3D nickel foam towards toluene oxidation. *Mol. Catal.* **2018**, *454*, 12–20. [CrossRef]

40. Luo, Y.; Zheng, Y.; Zuo, J.; Feng, X.; Wang, X.; Zhang, T.; Zhang, K.; Jiang, L. Insights into the high performance of Mn-Co oxides derived from metal-organic frameworks for total toluene oxidation. *J. Hazard. Mater.* **2018**, *349*, 119–127. [CrossRef]

41. Mo, S.; Li, S.; Li, W.; Li, J.; Chen, J.; Chen, Y. Excellent low temperature performance for total benzene oxidation over mesoporous CoMnAl composited oxides from hydrotalcites. *J. Mater. Chem. A* **2016**, *4*, 8113–8122. [CrossRef]

42. Mo, S.; Li, S.; Li, J.; Deng, Y.; Peng, S.; Chen, J.; Chen, Y. Rich surface Co(III) ions-enhanced Co nanocatalyst benzene/toluene oxidation performance derived from Co$^{II}$Co$^{III}$ layered double hydroxide. *Nanoscale* **2016**, *8*, 15763–15773. [CrossRef] [PubMed]

43. Xie, S.; Liu, Y.; Deng, J.; Yang, J.; Zhao, X.; Han, Z.; Zhang, K.; Dai, H. Insights into the active sites of ordered mesoporous cobalt oxide catalysts for the total oxidation of o -xylene. *J. Catal.* **2017**, *352*, 282–292. [CrossRef]

44. Wang, Y.; Guo, L.; Chen, M.; Shi, C. CoMn$_x$O$_y$ nanosheets with molecular-scale homogeneity: An excellent catalyst for toluene combustion. *Catal. Sci. Technol.* **2018**, *8*, 459–471. [CrossRef]

45. Tian, Z.-Y.; Tchoua Ngamou, P.H.; Vannier, V.; Kohse-Höinghaus, K.; Bahlawane, N. Catalytic oxidation of VOCs over mixed Co–Mn oxides. *Appl. Catal. B Environ.* **2012**, *117–118*, 125–134. [CrossRef]

46. Daté, M.; Okumura, M.; Tsubota, S.; Haruta, M. Vital Role of Moisture in the Catalytic Activity of Supported Gold Nanoparticles. *Angew. Chem. Int. Ed.* **2004**, *116*, 2181–2184. [CrossRef]

47. Wang, H.F.; Kavanagh, R.; Guo, Y.L.; Guo, Y.; Lu, G.Z.; Hu, P. Structural origin: Water deactivates metal oxides to CO oxidation and promotes low-temperature CO oxidation with metals. *Angew. Chem. Int. Ed.* **2012**, *51*, 6657–6661. [CrossRef]

48. Chen, B.-B.; Shi, C.; Crocker, M.; Wang, Y.; Zhu, A.-M. Catalytic removal of formaldehyde at room temperature over supported gold catalysts. *Appl. Catal. B Environ.* **2013**, *132–133*, 245–255. [CrossRef]